Proceedings of the ASME 2015 International Mechanical Engineering Congress & Exposition
IMECE2015
November 13-19, 2015, Houston, Texas, USA

IMECE2015-52631

VIRTUAL SIMULATION OF BLAST, BEHIND-ARMOR BLUNT TRAUMA, AND PROJECTILE PENETRATION LEADING TO INJURY OF LIFE-CRITICAL ORGANS IN THE HUMAN TORSO

Candice F. Cooper
Terminal Ballistics Technology
Sandia National Laboratories
Albuquerque, New Mexico, United States of America

Paul A. Taylor
Terminal Ballistics Technology
Sandia National Laboratories
Albuquerque, New Mexico, United States of America

ABSTRACT

Light body armor development for the warfighter is based on trial-and-error testing of prototype designs against ballistic projectiles. Torso armor testing against blast is virtually nonexistent but necessary to ensure adequate mitigation against injury to the heart and lungs. In this paper, we discuss the development of a high-fidelity human torso model and the associated modeling & simulation (M&S) capabilities. Using this torso model, we demonstrate the advantage of virtual simulation in the investigation of wound injury as it relates to the warfighter experience. Here, we present the results of virtual simulations of blast loading and ballistic projectile impact to the torso with and without notional protective armor. Our intent here is to demonstrate the advantages of applying a modeling and simulation approach to the investigation of wound injury and relative merit assessments of protective body armor.

Keywords: Torso, Blast, Personal Protective Equipment, Modeling & Simulation, Wound-Injury Mechanics

INTRODUCTION

To assess protection performance against ballistic projectiles, protective apparel is placed over ballistic clay and the projectiles are fired into the armor/clay target. The clay is meant to be representative of the human torso and the behind-armor deflection is the principal metric used to assess armor performance. Although this approach provides a coarse relative merit assessment of protection, it does not examine the behind-armor blunt trauma to crucial torso organs. To address this shortcoming, researchers have developed physical surrogate torso models possessing embedded pressure sensors and accelerometers measuring thoracic pressures and accelerations [1,2]. Physical surrogates have the potential to enhance our understanding of the wave mechanics that occurs within the thoracic cavity but are constrained to monitoring pressure and acceleration data at a limited number of locations in the torso. To supplement this effort, we have developed a modeling and simulation (M&S) capability for wound injury scenarios to the head, neck, and torso of the warfighter. We are beginning to use this toolset to investigate the consequences of, and mitigation against, blast exposure, blunt force impact, and ballistic projectile penetration that leads to damage of critical organs comprising the central nervous, cardiovascular, and respiratory systems. In this paper, we present the results of virtual simulations that investigate various injury scenarios using our newly-developed Sandia torso model as it is incorporated into the Sandia Eulerian shock wave physics code CTH [3]. This approach to understanding internal injury through M&S has a significant advantage over current methods by providing a virtual simulation capability to investigate wound injury mechanics and to optimize armor design without the need for extensive field testing. Also, M&S can be conducted ad infinitum without the use of human cadavers, animal testing, or expensive physical surrogates and the results can be interrogated in ways that are not easily measurable in physical experiments.

GEOMETRIC MODEL

The torso model is based on the National Library of Medicine's Visible Human male data set [4]. The model is constructed by segmenting 495 1 millimeter thick axially sliced

cryosections into the soft tissue, organs, and bone comprising the torso. The model begins at the base of the neck and continues to just superior to the pelvic region. Specifically, anatomically correct representations of 19 distinct materials including bone, cartilage, intervertebral discs, vasculature/blood, airways/air, lungs, liver, kidneys, spleen, heart, muscle, larynx, stomach, stomach contents, spinal cord, cerebrospinal fluid (CSF), thyroid, abdominal cavity contents, and skin/fat were created by segmenting the various tissues from the 495 axial slices. Our segmentation process preserved high anatomical fidelity and provides spatial resolution on the order of 1 mm (see Figure 1). The torso exists in both finite volume and finite element forms, consisting of roughly 42 million elements, for use with Eulerian, Lagrangian, or coupled Lagrangian-Eulerian codes. The dynamic mechanical response of each material comprising the torso is represented by a constitutive model that incorporates the most relevant material properties gathered from the scientific literature.

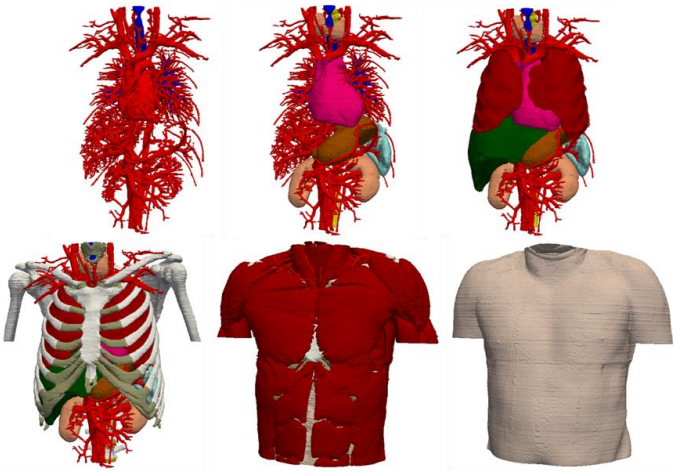

FIGURE 1. EVOLUTION OF TORSO MODEL DEVELOPMENT. TOP LEFT DISPLAYS BLOOD/VASCULATURE, AND AIR/AIRWAYS. TOP CENTER DISPLAYS THE ADDITION OF HEART, THYROID, SPINAL CORD AND CSF, SPLEEN, KIDNEYS, AND STOMACH. TOP RIGHT DISPLAYS THE ADDITION OF LUNGS AND LIVER. BOTTOM LEFT DISPLAYS THE ADDITION OF BONES, CARTILAGE, LARYNX, AND INTERVERTEBRAL DISCS. BOTTOM CENTER DISPLAYS ADDITION OF MUSCLE AND ABDOMINAL CAVITY CONTENTS. BOTTOM RIGHT DISPLAYS ADDITION OF SKIN/FAT.

The torso model is a continuation of the previously completed Sandia head-neck model [5] (see Figure 2). The Sandia head-neck model and Sandia torso model are both created from the National Library of Medicine's Visible Human male data set [4] with the torso model beginning where the head-neck model terminates. Because of this relation, the head-neck and torso models can be joined to create a complete head-neck-torso model if the need were to arise.

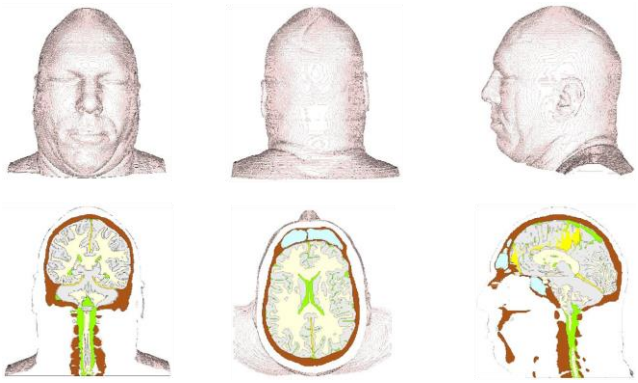

FIGURE 2: SANDIA HEAD-NECK MODEL.

CONSTITUTIVE MATERIAL MODELS

Our simulation method employs various equation-of-state (EOS) and constitutive models representing the 19 constituents of the torso model, the two materials comprising the chest plate model, the air enveloping the models (if blast loading is simulated), and the materials comprising projectiles and/or flying debris.

The constitutive models adopted for the torso model have been adapted from the constitutive models used in the head-neck model which have been described in detail in a previous publication [5] and therefore, are only briefly described here. The bone material is represented by a compressible, linear elastic perfectly plastic strength model and an accumulated strain-to-failure fracture model, fit to material properties data reported by Zhang et al. [6] and Carter [7] for cortical bone. The spinal cord is considered to be a compressible, viscoelastic material and is assigned model representations similar to those proposed by Zhang et al. [6]. Specifically, the spinal cord is represented by a Mie-Gruneisen [8], compressible equation-of-state model for the volumetric response and by a separate 3-term Maxwell viscoelastic model for the deviatoric (shear) response. These representations are described in detail for white matter by Taylor et al. [5]. The remaining soft tissues are represented by a Mie-Gruneisen equation-of-state (EOS) describing volumetric response and a linear elastic model describing deviatoric response. If inelastic response is anticipated, we use a von Mises plasticity model to represent the yield strength of the material. Blood, spinal fluid, and other body fluids are represented by a Tillotson-Brundage (T-B) equation-of-state model that accurately captures their respective bulk properties under compression and their susceptibility to fluid cavitation when subjected to isotropic tension (i.e. tensile pressure) [9,10]. The T-B equation-of-state representation for fluids requires the assignment of a tensile (negative) pressure at which cavitation is predicted to occur. For blood and spinal fluid, we have set the cavitation pressure at -150 kPa [11] and -100 kPa [12], respectively.

Our notional chest plate armor model consists of a Kevlar® hard shell backed by polyurethane foam padding. During blast loading, we expect these materials to remain elastic, and as such, have employed elastic model representations for these materials as defined by Nyein, et al. [13]. However, to simulate chest plate response to blunt impact and penetration, we must use constitutive model representations that capture the elastic, inelastic, and failure behavior of the hard shell and foam pad materials. In particular, we assume that the hard shell is a fiber-reinforced laminated composite and, as such, we represent the material using a transverse isotropic constitutive model [14].

Material Component	Volumetric Response	Deviatoric Response
Bone	Mie-Gruneisen EOS	Von Mises
Intervertebral Discs	Mie-Gruneisen	Von Mises
Costal Cartilage	Mie-Gruneisen	Von Mises
Larynx	Mie-Gruneisen	Von Mises
Vasculature/Blood	Tillotson-Brundage EOS	-
Airways/Air	Sesame Tabular EOS	-
Lungs	Mie-Gruneisen	Von Mises
Liver	Mie-Gruneisen	Von Mises
Kidneys	Mie-Gruneisen	Von Mises
Spleen	Mie-Gruneisen	Von Mises
Heart	Mie-Gruneisen	Von Mises
Muscle	Mie-Gruneisen	Von Mises
Stomach	Mie-Gruneisen	Von Mises
Stomach Contents	Tillotson-Brundage	-
Spinal Cord	Tillotson-Brundage	Viscoelastic
Cerebrospinal fluid	Tillotson-Brundage	-
Abdominal Cavity Contents	Mie-Gruneisen	Von Mises
Thyroid	Mie-Gruneisen	Von Mises
Skin	Mie-Gruneisen	Von Mises
Chest Plate	Mie-Gruneisen	Transverse-Isotropic
Chest Plate Padding	Mie-Gruneisen	Von Mises
9mm Projectile	Mie-Gruneisen	Steinberg-Guinan-Lund Plasticity [16]

TABLE 1: EOS AND STRENGTH MODEL DESCRIPTION FOR MATERIAL COMPONENTS

In order to simulate blast loading to the human torso model, air must be included in our simulations. Air envelops the model at ambient conditions, occupies the airways into and throughout the lungs, and transmits the blast waves. For this application, we have employed a non-linear, tabular equation-of-state representation for a dry air mix of N_2 (78.09%), O_2 (21.95%), and Ar (0.96%), reference density of 1.218e-3 g/cm^3, specifically designed for shock wave simulations [8].

SIMULATION METHODOLOGY

Blast and penetration simulations are performed using the shock wave physics code CTH [3]. CTH is an Eulerian finite-volume computer simulation code that is capable of tracking 90+ materials simultaneously, simulating their interactions as they undergo impact, blast loading, and penetration. This code adequately captures the fluid-solid interactions that occur between the pressurized air and the torso model. CTH possesses an extensive array of constitutive models with which to represent bone, biological tissue, projectile materials, and both the ambient and pressurized air used in our simulations.

Ideally, we would validate our torso model and simulation methodology against forensic wound data obtained from battlefield injuries due to blast and ballistic projectile impact. Since we are still in the process of collecting this data, our validation task has yet to be accomplished. With that said, we can still demonstrate our modeling and simulation approach to wound injury investigation and personal armor assessment. However, the reader is cautioned that the results we present here are for illustrative purposes and, at this time, are not meant to provide quantitative assessments of wound dynamics or armor assessment.

We conducted various simulations of direct blast exposure and projectile impact on our torso model both with and without the addition of notional body armor. For the purpose of testing the newly developed torso model, blast conditions were selected that were identical to those conditions used previously in simulations on the head-neck model [5]. These blast conditions are representative of conditions that a warfighter might experience during exposure to an IED detonation. We selected a blast history that would result from a spherical 2.3 kg charge of Composition-4 (C-4) located 2.3 meters from the torso model. This explosion produces an air blast of 260 kPa (2.6 bars) overpressure with a pulse width of 2.0 msec as it encounters the torso model.

To reduce computational overhead, we approximate the blast wave produced by a detonating explosive without explicitly including the detonation event in our simulations. In this case, we perform these simulations by positioning the torso model within an environment of air at ambient conditions. We create the blast wave by introducing a slab of energized air, located approximately 36 cm from the torso at time zero. The back face of the air slab is fixed by a rigid boundary whereas the boundary at the front face of the slab, closest to the torso model, is removed for times greater than zero. When this occurs, air mass flows from the energized slab, creating a pressure pulse that propagates in the direction of the torso model. The amplitude and pulse width of the blast wave is determined by setting the energized air to predefined conditions

of energy, pressure, and slab thickness. By the time the pressure pulse reaches the torso, its amplitude has degraded to a specified magnitude, in this case 360 kPa (260 kPa gauge pressure), displaying a blast pulse similar to the classical Friedlander waveform (see Figure 3) [16].

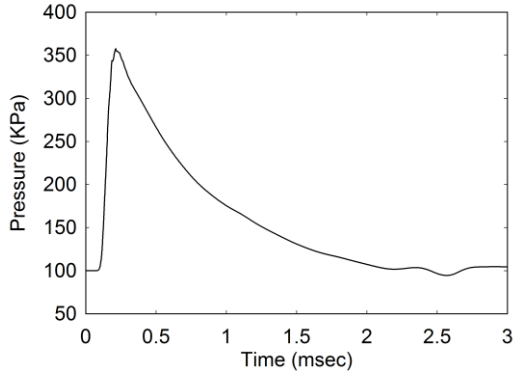

FIGURE 3: SIMULATED BLAST PULSE

Notional body armor was created to demonstrate the capability for relative merit assessment. The chest armor model is composed of a 1.0 cm thick Kevlar® shell in the blast simulations and a 1.5cm thick Kevlar® shell in the ballistic projectile impact simulations. The projectile used in these simulations is a mock representation of a 9 mm full metal jacket (FMJ) bullet. This representation captures the geometry and mass of a 9 mm FMJ bullet while simplifying its composition to that of a projectile composed of a single material.

DEMONSTRATION OF CHEST PLATE PERFORMANCE AGAINST BLAST LOADING

To assess the protective characteristics of a chest plate for a particular blast scenario, we simulate the event with the torso model wearing a chest plate backed with padding and compare those results with simulations of the same event with the torso model wearing a chest plate without padding as well as with the torso model unprotected. To assess protective efficacy of the various armor configurations, we monitor the maximum compressive and tensile pressures, maximum von Mises stress, and the prediction of cavitation.

As an example, Figures 4, 5, and 6, display the various armor configurations at the initial state of the frontal blast simulations. Figures 7 and 8 illustrate the predicted maximum compressive pressure generated within the torso and various life-critical organs in the unprotected configuration over the duration of the blast event. By evaluating the sagittal and axial sections it can be seen that the heart and lungs are subjected to relatively high compressive pressure. These plots suggest that the max pressure sustained in the heart and lungs is roughly twice that of the blast wave, i.e., 600-700 kPa.

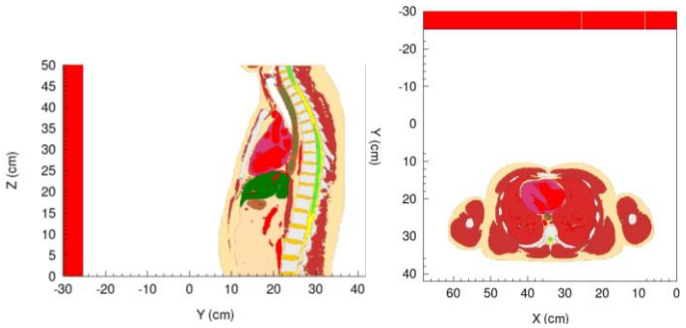

FIGURE 4: FRONTAL BLAST SIMULATION WITH NO ARMOR AT TIME ZERO. LEFT: SAGITTAL SECTION. RIGHT: AXIAL SECTION

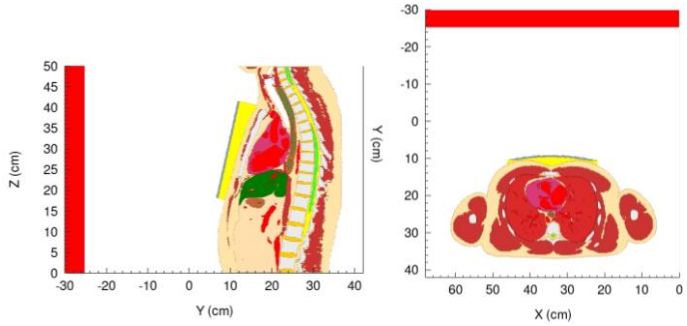

FIGURE 5: FRONTAL BLAST SIMULATION WITH ARMOR BACKED BY FOAM PADDING AT TIME ZERO. LEFT: SAGITTAL SECTION. RIGHT: AXIAL SECTION.

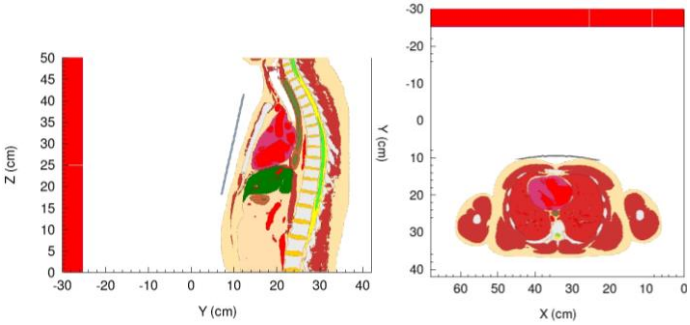

FIGURE 6: FRONTAL BLAST SIMULATION WITH ARMOR, WITHOUT FOAM PADDING, AT TIME ZERO. LEFT: SAGITTAL SECTION. RIGHT: AXIAL SECTION.

Figures 9 and 10 illustrate the predicted maximum von Mises stress generated within the torso and various life-critical organs throughout the duration of the blast event. It is useful to evaluate the von Mises stress as it provides an overall measure for the extent of shear stress that the tissues have experienced throughout the simulation. Shear stress, and hence von Mises stress, can cause tissue damage through distortion and tearing. By analyzing the sagittal and axial sections it can be seen that the outer boundaries of the heart, liver, and lungs, experience approximately 1-30kPa of von Mises stress. It is also worth noting that the lung tissue around the branching airways within the lungs experiences approximately 1-30kPa of von Mises stress as well.

Figure 11 illustrates the predicted maximum tensile pressure generated within the torso and various life-critical

organs throughout the duration of the blast event. Tensile pressures volumetrically dilate the tissues and have the potential to induce cavitation in the fluids. This is of great import when considering the fluids within the torso, such as the cerebrospinal fluid and blood. Under tension, these fluids are susceptible to cavitation [11,12]. Figures 12 and 13 illustrate the predicted maximum vapor fraction generated throughout the duration of the blast event. The maximum vapor fraction represents the maximum ratio of vapor volume to the total volume of each computational cell which has been predicted to undergo a phase change into vapor, as a result of cavitation, at any time throughout the simulation. This metric is useful in understanding where cavitation may be occurring and to what extent.

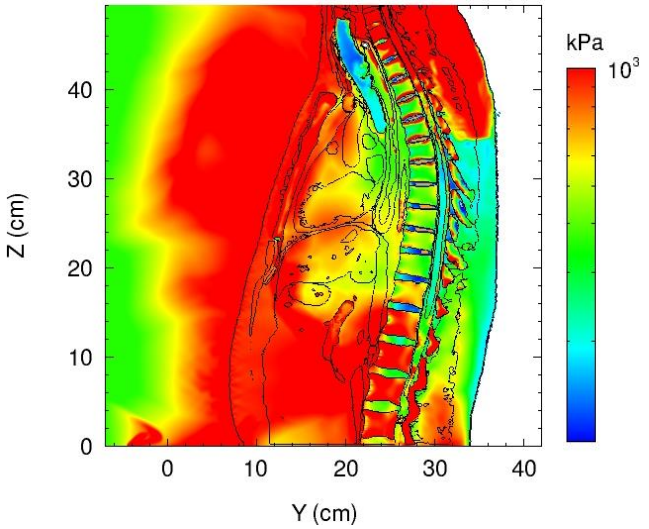

FIGURE 7: MAXIMUM COMPRESSIVE PRESSURE GENERATED THROUGHOUT FRONTAL BLAST SIMULATION ON TORSO WITHOUT ARMOR. SAGITTAL SECTION.

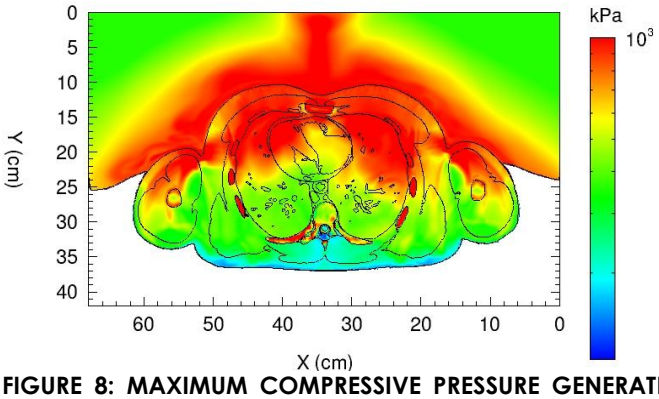

FIGURE 8: MAXIMUM COMPRESSIVE PRESSURE GENERATED THROUGHOUT FRONTAL BLAST SIMULATION ON TORSO WITHOUT ARMOR. AXIAL SECTION.

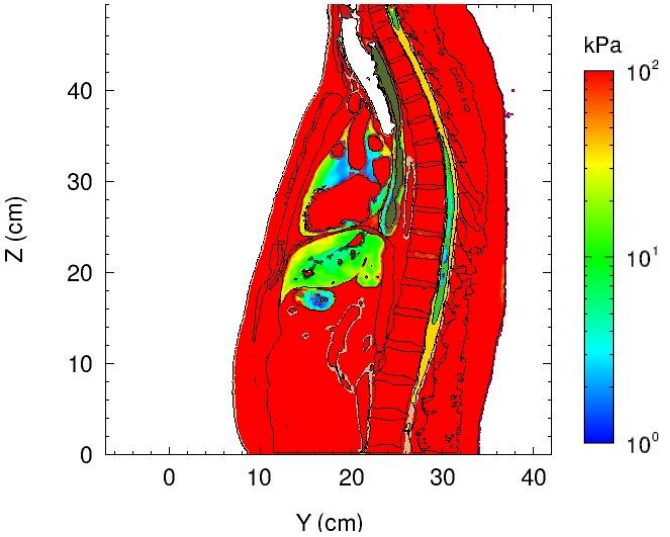

FIGURE 9: MAXIMUM VON MISES STRESS GENERATED THROUGHOUT FRONTAL BLAST SIMULATION ON TORSO WITHOUT ARMOR. SAGITTAL SECTION.

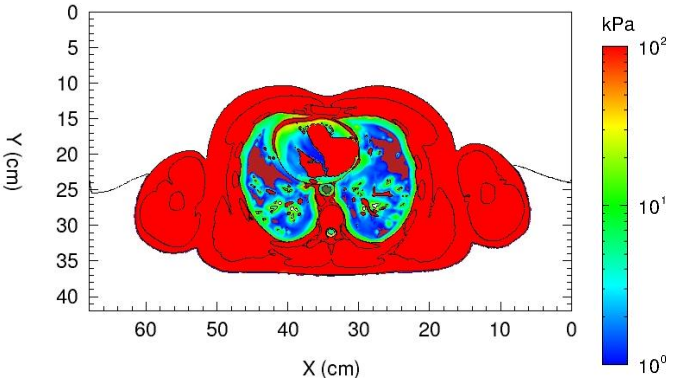

FIGURE 10: MAXIMUM VON MISES STRESS GENERATED THROUGHOUT FRONTAL BLAST SIMULATION ON TORSO WITHOUT ARMOR. AXIAL SECTION.

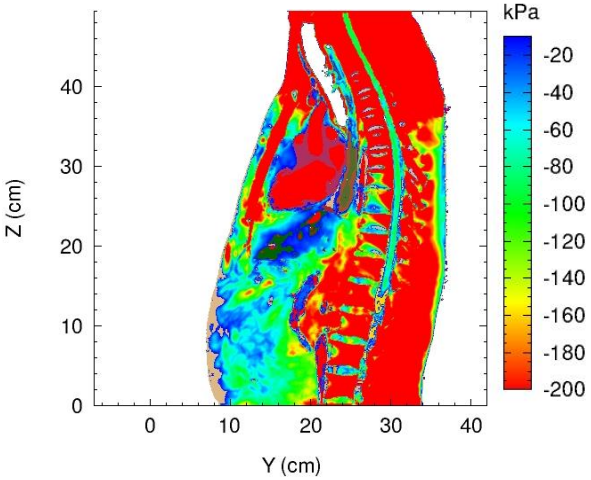

FIGURE 11: MAXIMUM TENSILE PRESSURE GENERATED THROUGHOUT FRONTAL BLAST SIMULATION ON TORSO WITHOUT ARMOR. SAGITTAL SECTION.

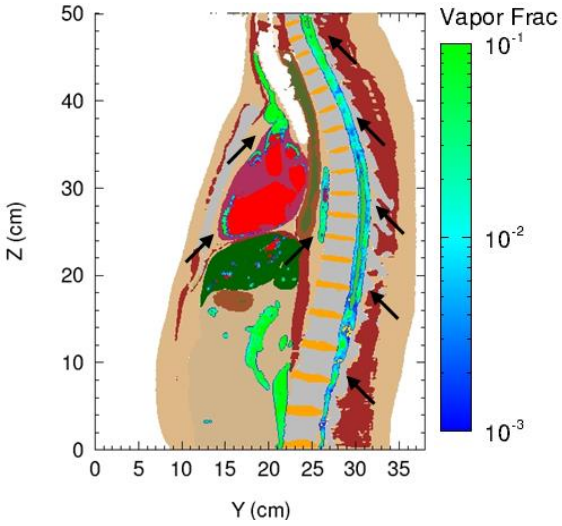

FIGURE 12: MAXIMUM VAPOR VOLUME FRACTION GENERATED THROUGHOUT FRONTAL BLAST SIMULATION ON TORSO WITHOUT ARMOR. SAGITTAL SECTION. ARROWS POINT TOWARD AREAS OF PREDICTED CAVITATION.

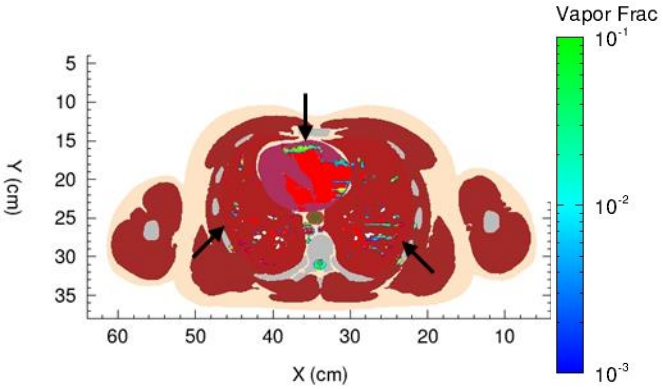

FIGURE 13: MAXIMUM VAPOR VOLUME FRACTION GENERATED THROUGHOUT FRONTAL BLAST SIMULATION ON TORSO WITHOUT ARMOR. AXIAL SECTION. ARROWS POINT TOWARD AREAS OF PREDICTED CAVITATION.

It is useful to look at specific points within the torso for comparative analysis. Figure 14-17 show the history plots of tracers placed within the heart, right lung, left lung, and liver. These plots show the pressure histories at those points throughout the simulations. Note that the addition of armor creates various changes in the pressures seen within the heart, lungs, and liver. It can be seen that the addition of armor, with or without padding, creates an increase in the peak pressures within the heart and liver over the protected case. However, the increase in peak pressure within the heart and liver coincides with a decrease in loading rate. This increase in peak pressure is not seen in the lungs. Figures 16 and 17 show that the armor with padding does not change the pressure magnitude or its rate of loading in the lungs; however, there is an extension in the pulse width over that for the unprotected torso. The armor without padding decreases the peak pressure magnitudes in the lungs; however, there is an extension in the pulse width, even beyond that for the armor with padding.

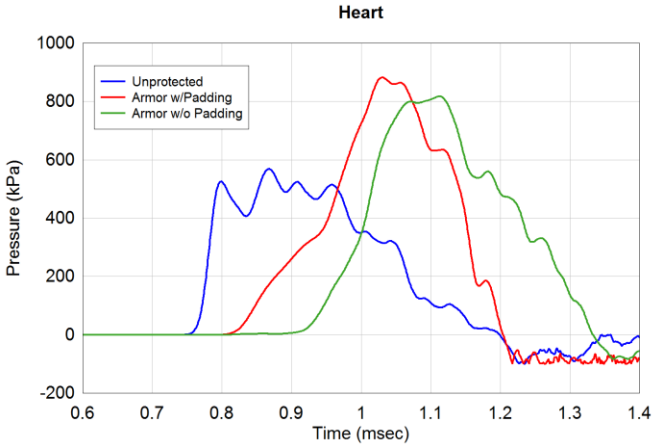

FIGURE 14: PRESSURE HISTORY AT A TRACER POINT PLACED WITHIN THE HEART.

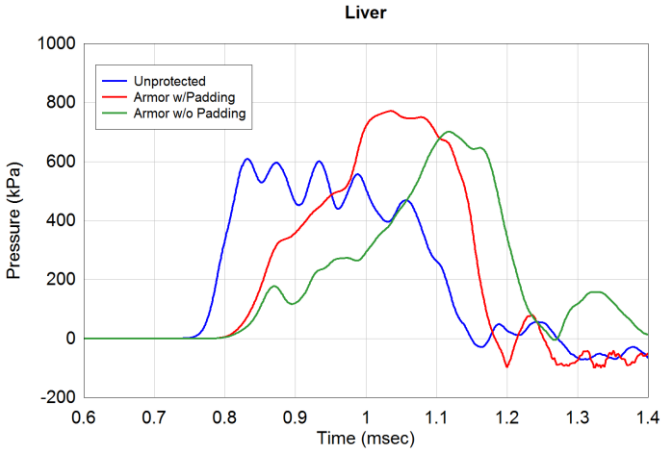

FIGURE 15: PRESSURE HISTORY AT A TRACER POINT PLACED WITHIN THE LIVER.

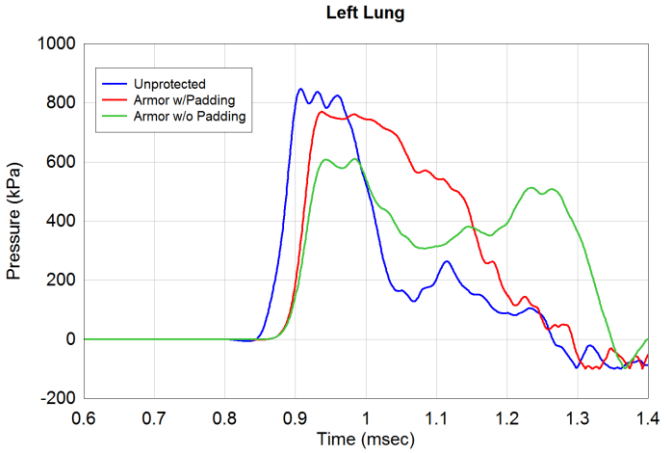

FIGURE 16: PRESSURE HISTORY AT A TRACER POINT PLACED WITHIN THE LEFT LUNG.

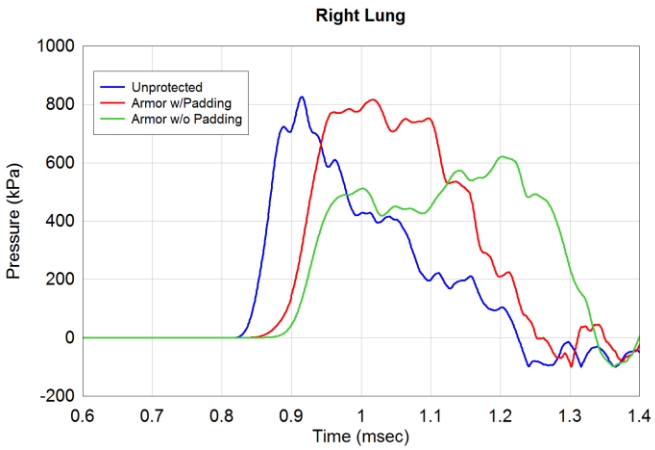

FIGURE 17: PRESSURE HISTORY IN A TRACER POINT PLACED WITHIN THE RIGHT LUNG.

DEMONSTRATION OF CHEST PLATE PERFORMANCE AGAINST PROJECTILE PENETRATION

Our modeling and simulation toolset can also be utilized to evaluate armor performance against projectile impact and in the assessment of behind-armor blunt trauma. To demonstrate this capability, we equip the torso model with a notional armor chest plate backed by padding (see Figure 18). The torso model was subjected to a ballistic impact with a projectile velocity of 370 m/s. To access protective efficacy, we can again monitor the maximum compressive and tensile pressures, maximum von Mises stress, and the prediction of cavitation. In this simulation, maximum tensile pressures within the blood and cerebrospinal fluid did not surpass the threshold for cavitation and as such the graphical interpretation of cavitation is of no value.

Figures 19 and 20 illustrate the maximum compressive pressure generated throughout the projectile impact simulation. It can be seen from the sagittal and axial sections that the heart and lungs are subject to relatively high compressive pressures on the order of 500-1000kPa in some areas.

Figures 21 and 22 illustrate the maximum von Mises stress generated throughout the projectile impact simulation. By evaluating the sagittal and axial sections, it can be seen that portions of the heart, lungs, and liver experience von Mises stress roughly between 1 and 30kPa.

Figures 23 and 24 illustrate the maximum tensile pressure generated throughout the projectile impact simulation. By evaluating the sagittal and axial sections, it can be seen that portions of the heart and lungs are subject to relatively high tensile pressures. It is also important to notice that there is not significant tensile pressure in the blood or cerebrospinal fluid which explains why there is no prediction of cavitation in this case.

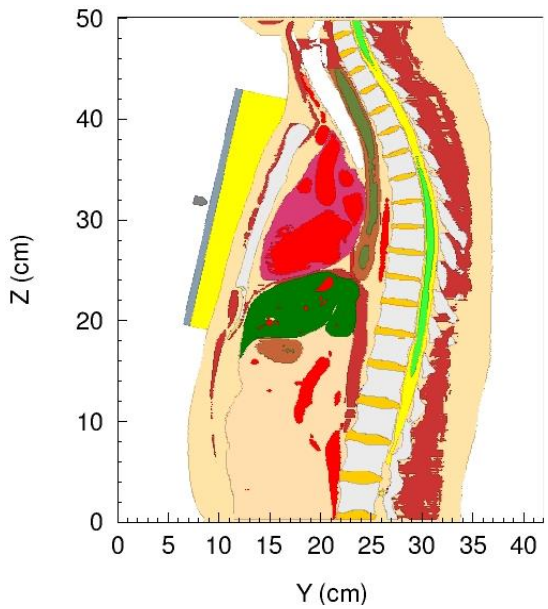

FIGURE 18: PROJECTILE IMPACT SIMULATION AT TIME ZERO.

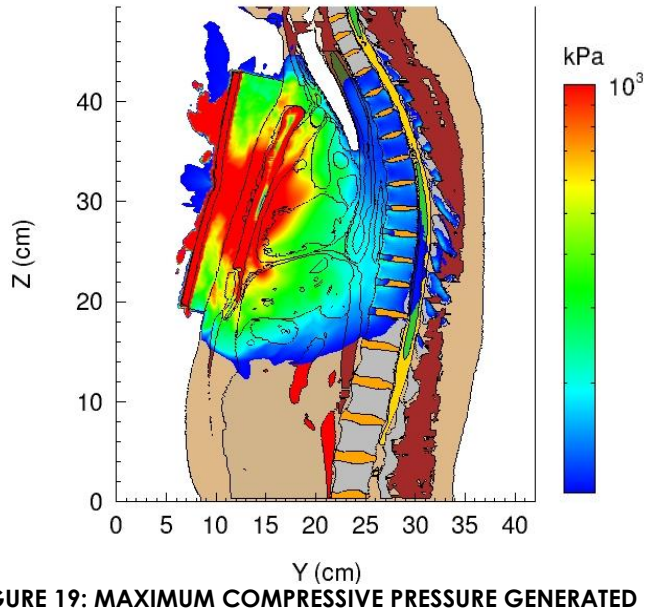

FIGURE 19: MAXIMUM COMPRESSIVE PRESSURE GENERATED THROUGHOUT PROJECTILE IMPACT SIMULATION. SAGITTAL SECTION.

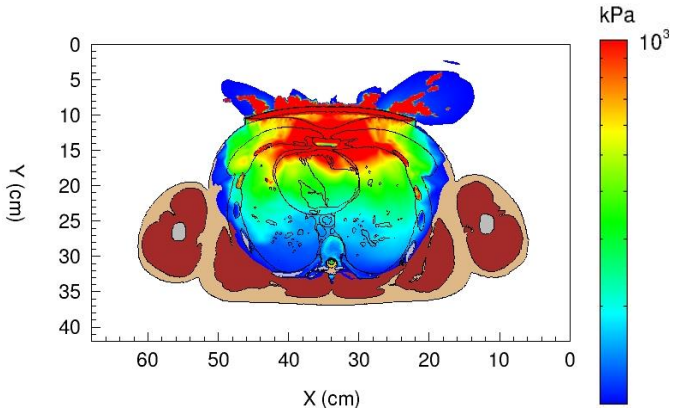

FIGURE 20: MAXIMUM COMPRESSIVE PRESSURE GENERATED THROUGHOUT PROJECTILE IMPACT SIMULATION. AXIAL SECTION.

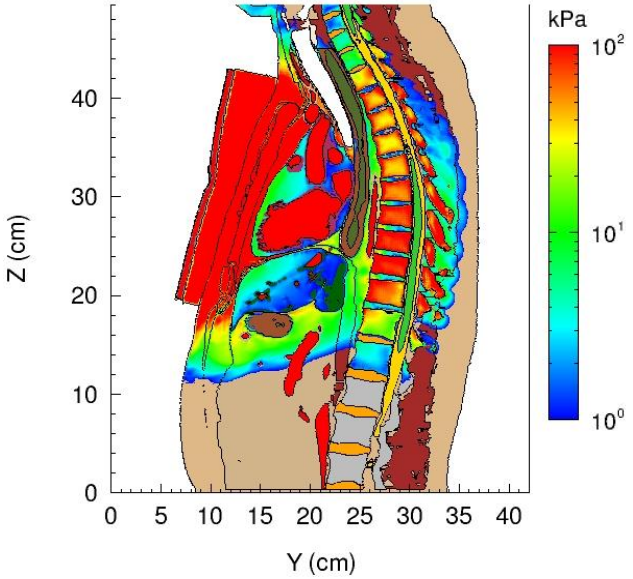

FIGURE 21: MAXIMUM VON MISES STRESS GENERATED THROUGHOUT PROJECTILE IMPACT SIMULATION. SAGITTAL SECTION.

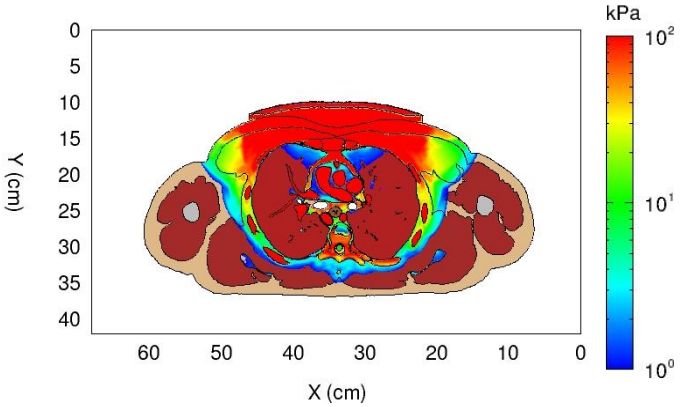

FIGURE 22: MAXIMUM VON MISES STRESS GENERATED THROUGHOUT PROJECTILE IMPACT SIMULATION. SAGITTAL SECTION.

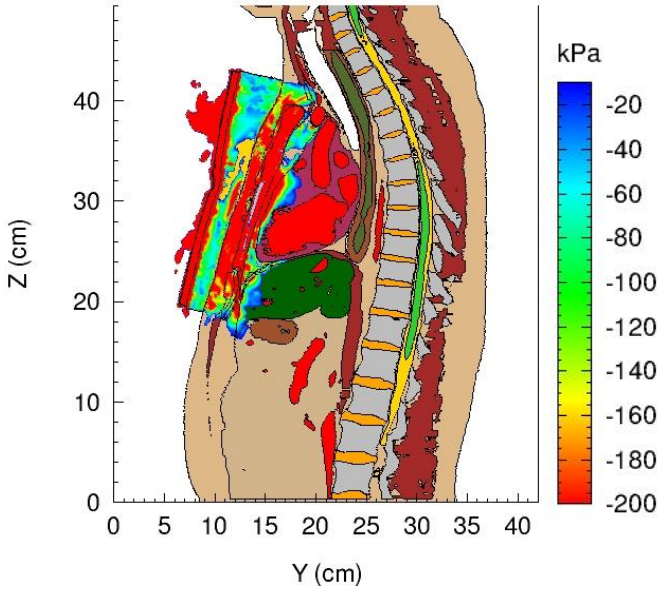

FIGURE 23: MAXIMUM TENSILE PRESSURE GENERATED THROUGHOUT PROJECTILE IMPACT SIMULATION. SAGITTAL SECTION.

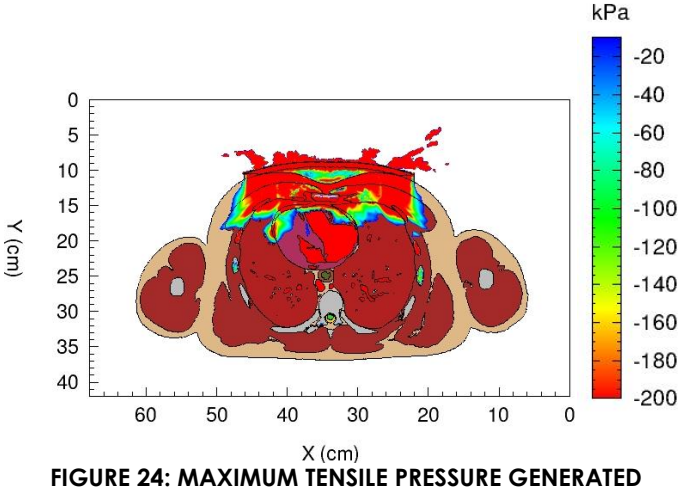

FIGURE 24: MAXIMUM TENSILE PRESSURE GENERATED THROUGHOUT PROJECTILE IMPACT SIMULATION. AXIAL SECTION.

DISCUSSION

By validating the model against available related forensic wound data, we will be able to identify variables such as pressure, von Mises stress, deviatoric or volumetric strain energies, and cavitation that correlate with various wound injury mechanics. This in turn will allow us to utilize our M&S capabilities in assessing wound injury mechanisms and conducting relative merit assessments of PPE. In the current state, it is still useful to evaluate the simulation results and make qualitative comparisons.

Pressure alone is not necessarily indicative of tissue damage; it is, however, a valuable metric in assessing relative differences between the various armor configurations and

simulation events, such as blast impact or projectile impact. Under the assumption that maximum peak pressure is correlated with tissue damage, it could be said that the addition of the chest plate with padding under blast impact is deleterious to the heart and liver, and does not create a significant change in peak pressure in the lungs relative to an unprotected configuration. Under the same assumption, the addition of the chest plate without padding under blast impact is deleterious to the heart and liver; however, it provides protection in the form of a decrease in peak pressure to the lungs.

If instead, the assumption was made that the pressure load rate is correlated with tissue damage, it could be said that the addition of the chest plate both with and without padding under blast impact decreased the pressure load rate in the heart and liver, thus providing a protective quality to these organs and remained nearly unchanged in the lungs relative to an unprotected configuration.

Further study and validation of the correlation between peak pressure or pressure load rate and tissue damage is necessary in order to draw any concise conclusions from the results. Once these correlations are established, these variables will be valuable in assessing armor design and conducting optimization studies.

CONCLUSION

In this paper, we have attempted to demonstrate the advantages of employing high fidelity simulation methods over methods relying exclusively on laboratory and field testing in the analysis of wound injury mechanics and relative armor assessments. Once a digital human model or armor model has been created, it can be virtually tested ad infinitum without the necessary use of cadavers, physical surrogate models, or the destruction of the PPE employed in the study. Furthermore, one may alter the constitutive properties of one or more materials (equivalent to changing the materials themselves) in the digital PPE model and resume further virtual testing to assess the benefits of the alteration and provide insights for optimization.

It is not the case that this work is intended to completely replace laboratory and field testing. Rather, a modeling and simulation effort ought to be used in collaboration with, and validated against, laboratory and field test data in order to provide the most benefit to the wound injury mechanics and PPE development communities. In this way, modeling and simulation can play a role in PPE development by reducing expensive field testing and possibly revealing novel design concepts that may otherwise have been overlooked by an exclusive test-and-evaluation approach.

Additional studies including simulations with various blast directions have been conducted, however, they have been omitted here for the sake of brevity.

ACKNOWLEDGMENTS

The authors acknowledge the National Library of Medicine and the Visible Human Project as the source of the Visible Human Data Set used to construct the digital torso and head-neck models employed in this research. This work is funded by the laboratory-directed research and development (LDRD) program at Sandia National Laboratories. Sandia National Laboratories is a multi-program laboratory managed and operated by Sandia Corporation, a wholly owned subsidiary of Lockheed Martin Corporation, for the United States Department of Energy's National Nuclear Security Administration under contract DE-AC04-94AL85000.
SAND2015-3337 C

REFERENCES

[1] Roberts, J. C., Biermann, P. J., O-Connor, J. V., Ward, E. E., Cain, R. P., Carkhuff, B. G., Merkle, A. C., 2005, "Modeling Nonpenetrating Ballistic Impact on a Human Torso," Johns Hopkins APL Technical Digest, **26**(1), 84-92.

[2] Roberts, J. C., Merkle, A. C., Biermann, P. J., Ward, E. E., Carkhuff, Cain, R. P., O-Connor, J. V., 2007, "Computational and experimental models of the human torso for non-penetrating ballistic impact, J. Biomech. **40**, 125-136.

[3] Hertel, E. S., Bell, R., Elrick, M., Farnsworth, A., Kerley, G., McGlaun, J., Petney, S., Silling, S., and Taylor, P., 1993, "CTH: a software family for multi-dimensional shock physics analysis," Proc. 19th Int. Symp. Shock Waves, **1**, pp. 377–382.

[4] National Institutes of Health, 2007, "The Visible Human Project," National Library of Medicine, http://www.nlm.nih.gov/research/visible/visible_human.html.

[5] Taylor, P. A., Ludwigsen, J. S., and Ford, C. C., 2014, "Investigation of blast-induced traumatic brain injury," Brain Inj., **28**(7), pp. 879–895.

[6] Zhang, L., Yang, K. H., and King, A. I., 2001, "Comparison of brain responses between frontal and lateral impacts by finite element modeling," J. Neurotrauma, **18**(1), pp. 21–30.

[7] Carter, D. R., 1984, Biomechanics of bone, Appleton & Lange.

[8] Hertel, E. S., and Kerley, G. I., 1998, CTH reference manual: The equation of state package, Sandia National Laboratories, Albuquerque, NM.

[9] Brundage, A. L., 2013, "Implementation of Tillotson equation of state for hypervelocity impact of metals, geologic materials, and liquids," Procedia Eng., **58**, pp. 461–470.

[10] Brundage, A. L., 2014, "Prediction of Shock-Induced Cavitation in Water," J. Physics: Conference Series **500**, 102002.

[11] Williams, J. C., Woodward, J. F., Stonehill, m. A., Evan, A. P., McAteer, J. A., 1999, "Cell damage by lithotripter shock waves at high pressure to preclude cavitation," Ultrasound in Med. & Biol., 25(9), 1445-1449.

[12] Brundage, A., L., 2014, personal communication.

[13] Nyein, M. K., Jason, A. M., Yu, L., Pita, C. M., Joannopoulos, J. D., Moore, D. F., and Radovitzky, R.A., 2010, "In silico investigation of intracranial blast mitigation with relevance to military traumatic brain injury," Proc. Natl. Acad. Sci., **107**(48), pp. 20703–20708.

[14] Taylor, P.A., 1995, "CTH Reference Manual: The Transverse Isotropic (TI) Model," Sandia National Laboratories report SAND95-2750.

[15] Steinberg, D. J., Cochran, S. G., and Guinan, M. W., 1980, "A constitutive model for metals applicable at high-strain rate," J. Appl. Phys. **51**, 1498.

[16] Friedlander, F. G., 1947, "Simple progressive solutions of the wave equation," Math. Proc. Camb. Philos. Soc., **43**(3), pp. 360–373.

